

# Protostars, Dust Globules, and a Herbig-Haro Object in the LMC Superbubble N 51D

Y.-H. Chu<sup>1</sup>, R. A. Gruendl<sup>1</sup>, C.-H. R. Chen<sup>1</sup>, B. A. Whitney<sup>2</sup>, K. D. Gordon<sup>3</sup>, L. W. Looney<sup>1</sup>, G. C. Clayton<sup>4</sup>, J. R. Dickel<sup>1</sup>, B. C. Dunne<sup>1</sup>, S. D. Points<sup>5</sup>, R. C. Smith<sup>5</sup>, and R. M. Williams<sup>1</sup>

## ABSTRACT

Using *Spitzer Space Telescope* and *Hubble Space Telescope* observations of the superbubble N51D, we have identified three young stellar objects (YSOs) in dust globules, and made the first detection of a Herbig-Haro object outside the Galaxy. The spectral energy distributions of these YSOs suggest young massive stars with disk, envelope, and outflow cavities. The interstellar conditions are used to assess whether the star formation was spontaneous or induced by external pressure.

*Subject headings:* Magellanic Clouds — HII regions — ISM: individual (N51)

## 1. Introduction

The *Spitzer Space Telescope*, with its high angular resolution and sensitivity in the mid- and far-infrared wavelengths, opens a new window to view the formation of individual massive stars not only in the Galaxy but also in nearby galaxies, such as the Large Magellanic Cloud (LMC). Using *Spitzer* observations, Jones et al. (2005) reported four young stellar objects (YSOs) in the H II complex N 159 in the LMC. We have obtained *Spitzer* observation of the superbubble LH $\alpha$  120-N 51D (designation from Henize 1956), or N 51D for short, in the LMC, and are surprised to find YSOs projected within the superbubble where the density is expected to be low.

---

<sup>1</sup>Astronomy Department, University of Illinois, 1002 W. Green Street, Urbana, IL 61801

<sup>2</sup>Space Science Institute, 4750 Walnut Street, Suite 205, Boulder, CO 80301.

<sup>3</sup>Steward Observatory, University of Arizona, Tucson, AZ 85721

<sup>4</sup>Department of Physics and Astronomy, Louisiana State University, Baton Rouge, LA 70803

<sup>5</sup>Cerro Tololo Inter-American Observatory, Casilla 603, La Serena, Chile

N 51D has been partially imaged with the *Hubble Space Telescope* (*HST*) in the  $H\alpha$  and [S II] lines (Chen et al. 2000). These *HST* images allow us to identify dust globules and Herbig-Haro (HH) objects associated with YSOs. We have modeled the spectral energy distributions (SEDs) of these YSOs in dust globules to estimate their physical parameters. We have further used  $H\alpha$  and X-ray observations to determine the external gas pressure of the dust globules, in order to assess whether the star formation was spontaneous or induced. This *Letter* reports our analysis of *Spitzer* and *HST* observations of the three YSOs embedded in dust globules in N 51D.

## 2. Observations and Data Reduction

Our *Spitzer* observations of N 51D were made with the Infrared Array Camera (IRAC; Fazio et al. 2004) on 2004 December 16 and the Multiband Imaging Photometer for *Spitzer* (MIPS; Rieke et al. 2004) on 2005 April 3. The IRAC observations were obtained using the mapping mode to cover a  $\sim 30' \times 20'$  area in the 3.6, 4.5, 5.8, and 8.0  $\mu\text{m}$  bands. The four band maps overlap in a smaller region,  $\sim 23' \times 20'$  in size. Each position in the map was observed with five 30 s integrations taken in the high dynamic range mode and using medium dithers in a cyclic pattern between exposures to aid in the rejection of transients. The resulting integration time at each location in the image was  $\sim 150$  s. Our analyses use the post-BCD (Basic Calibrated Data) products resulting from standard pipeline processing (version S11.0.2).

The MIPS observations were obtained using the scan map mode in the 24, 70, and 160  $\mu\text{m}$  bands. The medium scan rate was used to map a region comprised of sixteen  $0.5^\circ$  scan legs with a cross-scan step of  $148''$  to cover a region  $30' \times 20'$  in all three MIPS bands. The MIPS DAT v3.00 (Gordon et al. 2005) was used to do the basic processing and final mosaicking of the individual images. In addition, extra processing steps on each image were carried out. At 24  $\mu\text{m}$ , these include readout offset correction and division by a scan-mirror-independent flat field. At 70 and 160  $\mu\text{m}$  the extra step was a pixel-dependent background subtraction for each map (using a low-order polynomial fit to the source free regions). The final mosaics have exposure times of roughly 200, 80, and 18 s  $\text{pixel}^{-1}$  for 24, 70, and 160  $\mu\text{m}$ , respectively. The MIPS photometry was determined using the point source fitting software StarFinder (Diolaiti et al. 2000) and a smoothed STinyTim model point spread function.

### 3. YSOs in the Superbubble N 51D

#### 3.1. Identification of YSOs

YSOs can be distinguished from normal stars because of their excess infrared emission from circumstellar dust. To show the locations of YSOs and normal stars with respect to the ionized interstellar gas, we present in Figure 1a a color composite of IRAC  $8\ \mu\text{m}$  (red), optical continuum at  $5000\ \text{\AA}$  (blue), and  $\text{H}\alpha$  (green) images. In this color image, the ionized interstellar gas appears green and diffuse, most normal stars appear blue and unresolved, YSOs appear red and unresolved, and the interstellar dust emission appears red and diffuse.

The ionized gas shell of the superbubble N 51D is elongated along the N-S direction with a faint extension to the southwest. The  $8\ \mu\text{m}$  diffuse dust emission is the brightest in filaments along the periphery of the ionized gas shell; it also shows a faint component extending across the entire field. Two OB associations, LH 51 and LH 54 (Lucke & Hodge 1970; Oey & Smedley 1998), exist within the superbubble, appearing as concentrations of blue stars near the western and eastern shell rims in Figure 1a. Bright YSOs are seen within the boundary of the N 51D superbubble. Some YSOs along the north and west shell rims are associated with bright filamentary dust emission, while the other YSOs appear isolated. Some YSOs are projected within the OB associations LH 51 and LH 54, but the YSOs on the north rim are not near either association.

Note however that not all red stars in Figure 1a are YSOs. These red stars may appear red or blue in the color composite of IRAC  $3.6$ ,  $4.5$ , and  $8.0\ \mu\text{m}$  images displayed in Figure 1b. To determine the nature of these stars, we examine their colors quantitatively and present an IRAC color-color diagram ( $[3.6]-[4.5]$  versus  $[5.8]-[8.0]$ ) and a color-magnitude diagram ( $[8.0]$  versus  $[3.6]-[8.0]$ ) of N 51D in Figure 2. Similar diagrams presented by Allen et al. (2004) and Whitney et al. (2004) for star forming regions show that normal stars have zero colors and that YSOs exhibit a range of red colors depending on their classes, or amounts of circumstellar material. For the color schemes we use, YSOs appear red in both Figures 1a and 1b, but normal stars appear blue in Figure 1b even if they appear red in Figure 1a.

We use the objects 1-4 marked in Figures 2 and 3 as examples. Objects 1-3 are YSOs and they appear red in both Figures 1a and 1b. Object 4 has been cataloged as L54S-81 with  $V = 16.82 \pm 0.01$ ,  $(B - V) = 1.67 \pm 0.05$  (Oey 1996), and  $K = 11.64 \pm 0.02$  (2MASS). Its colors and magnitudes are consistent with a Galactic M4 V star at a distance of 67 pc; thus star 4 appears blue in Figure 1b and shows nearly zero colors in Figure 2a.

### 3.2. Dust Globules and Herbig-Haro Object

The eastern rim of the N 51D superbubble has been imaged by the *HST* WFPC2 in the  $H\alpha$  and [S II]  $\lambda\lambda 6716, 6731$  lines (Chen et al. 2000). Figure 3a shows a color composite of the *HST*  $H\alpha$  (green) and [S II] (blue) images and *Spitzer* 8  $\mu\text{m}$  image (red). While the foreground M dwarf (object 4 in Fig. 2) appears isolated, the three YSOs (objects 1–3 in Fig. 2) are each associated with a small dust feature whose surface gas is ionized.

Figure 3b shows a close-up  $H\alpha$  image of the dust globules associated with YSO-1 and YSO-2. The dust globules are each about  $5''$  in size, corresponding to 1.25 pc, slightly larger than typical Bok globules in the Galaxy and in the LMC (Clemens et al. 1991; Garnett et al. 1999). The bright star to the east of YSO-2 is the WR star HD 36402 (Breysacher, Azzopardi, & Testor 1999).

The dust feature associated with YSO-3, shown in Figure 3c, has a different morphology. Its surface toward the center of the N 51D superbubble is photoionized, but its back side is not. The [S II] close-up in Figure 3d shows additional knots of emission extending from the north rim outward along an almost straight line. These knots are faint in  $H\alpha$ . Their [S II]/ $H\alpha$  ratios increase outward from 0.5 to 0.65, significantly higher than those of the photoionized surface of the dust feature,  $0.25 \pm 0.05$ . The alignment of these knots and their high [S II]/ $H\alpha$  ratios are characteristics that are frequently seen in HH objects (Reipurth & Bally 2001); thus we suggest that *this is first HH object detected in the LMC*.

### 3.3. Physical Properties of the YSOs

We have measured the flux densities of the three YSOs in N 51D in all IRAC and MIPS bands, and listed them in Table 1. The SEDs were modeled with a 2-D radiation transfer code appropriate for YSOs (Whitney et al. 2003). These models include thermal dust emission but not PAH emission. The circumstellar geometry consists of any combination of a rotationally flattened envelope, flared disk, and bipolar cavities. YSO-1 is fit with a source luminosity of  $10,500 L_{\odot}$  appropriate for a B2–B3 main sequence star, an envelope infall rate of  $2 \times 10^{-4} M_{\odot} \text{ yr}^{-1}$ , disk mass of  $0.1 M_{\odot}$ , and bipolar outflow cavity opening angle of  $15^{\circ}$ . The disk and envelope centrifugal radius is 300 AU. These model parameters suggest a fairly young protostar. The disk radius could be varied by 50% and, with minor variations in other parameters, result in a similar SED. The total envelope mass is  $\sim 700 M_{\odot}$ , but this is somewhat dependent on our choice of outer radius and the radial density power law. The disk mass is also uncertain since the long-wavelength contribution blends with the envelope. However, without a disk, the envelope would have a steeper density profile and

less near- and mid-IR flux density. Our best model SED for YSO-1 is shown in Figure 4. Ten inclinations are shown, and the best-fit inclination is  $\sim 50^\circ$ .

YSO-2 is fit by a similar model as YSO-1: an illuminating B3 star ( $2500 L_\odot$ ), an envelope mass of  $\sim 210 M_\odot$  and infall rate of  $4 \times 10^{-4} M_\odot \text{ yr}^{-1}$ , disk mass of  $0.1 M_\odot$  and radius of 300 AU, and bipolar outflow cavity opening angle of  $30^\circ$ . The best-fit inclination is  $\sim 60^\circ$ .

YSO-3 is interesting because it requires a massive envelope to fit the long-wavelength SED, but a nearly unextinguished line of sight to the illuminating central source, suggested by the optical data available for this source (see Fig. 4; Zaritsky et al. 2002). We fit this with a  $\sim$ B4 star ( $1200 L_\odot$ ), envelope mass of  $\sim 230 M_\odot$  and infall rate of  $5 \times 10^{-4} M_\odot \text{ yr}^{-1}$ , disk mass of  $0.2 M_\odot$  and radius 400 AU, and bipolar cavity opening angle of  $40^\circ$ . The best fit inclination is  $\sim 40^\circ$ . This suggests either an evolved protostar with a substantial envelope and a large cavity carved out by outflows; or more than one source in the beam, an unextinguished source surrounded by a disk, and an embedded source with sufficient envelope mass to fit the long-wavelength SED. In either case, the model requires substantial warm dust, such as from a disk, to fit the mid-IR flux density. In the latter case, the HH object could come from either source.

In all of these sources, PAH emission in the [3.6], [4.5], and [8.0] IRAC bands is likely to contribute additional flux densities over the thermal emission accounted for by the models. This is especially true in YSO-3 which is less embedded than the other two sources. We have thus excluded these bands in estimating the best-fit inclination.

#### 4. Spontaneous or Induced Star Formation?

The three dust globules that harbor YSOs in N 51D are exposed to the radiation field of OB associations, similar to the dust pillars in the Eagle Nebula (Hester et al. 1996). The interstellar medium in N 51D has been well-studied, so we can use the external conditions of the dust globules to assess whether the star formation was induced by external pressure.

The interior of a superbubble is expected to be filled with shock-heated gas at  $10^6$ – $10^7$  K (Chu et al. 1995). The existence of hot gas in N 51D has been confirmed by the diffuse X-ray emission detected by *Einstein* and *ROSAT* (Chu & Mac Low 1990; Dunne, Points, & Chu 2001). Recent *XMM-Newton* observations provide high-quality X-ray spectra, and the best-fit thermal plasma emission models indicate that N 51D’s interior hot gas has an electron temperature of  $\sim 2.6 \times 10^6$  K and an electron density of  $\sim 0.03 \text{ cm}^{-3}$  (Cooper et al. 2004). The thermal pressure of this hot gas is  $P/k \sim 1.5 \times 10^5 \text{ cm}^{-3} \text{ K}$ , assuming a He to H number ratio of 1:10.

The ionized gas enveloping the dust globule around YSO-1 has a peak  $H\alpha$  surface brightness of  $1.4 \times 10^{-14}$  ergs  $s^{-1}$   $cm^{-2}$   $arcsec^{-2}$  along its limb-brightened rim, corresponding to an emission measure of  $6740$   $cm^{-6}$  pc for a temperature of  $10^4$  K. The ionized gas has a shell structure, and the longest path viewed through the shell is along the rim and equals  $2^{3/2}R(\Delta R/R)^{1/2}$ , where  $R$  and  $\Delta R$  are the shell radius and thickness, respectively. For a radius of  $0.65$  pc and a thickness of  $0.15$  pc (measured from the  $H\alpha$  image), the peak emission measure leads to an electron density of  $90 \pm 10$   $cm^{-3}$ . As the temperature of a photoionized gas is of order  $10^4$  K, the thermal pressure of the ionized skin of the dust globule is  $P/k \sim 2 \times 10^6$   $cm^{-3}$  K, substantially higher than that of N 51D’s interior hot gas.

The thermal pressure in the dust globule is  $P/k \sim 10^4$   $cm^{-3}$  K, assuming typical values of density ( $10^3$   $H_2$   $cm^{-3}$ ) and temperature (10 K) for Bok globules. This pressure is much lower than those of the ionized surfaces or the surrounding hot gas. The radii of the dust globules are slightly larger than the Jeans radius of  $0.5$  pc, implying that spontaneous collapse may have started the star formation. However, their co-location with the  $\sim 3$  Myr old OB association LH 54 (Oey & Smedley 1998) suggests that star formation in the globules is delayed and may have been induced recently by the thermal pressure of the superbubble interior. Assuming additional magnetic support, the magnetic pressure in the dust globules would be  $\lesssim 4$  times the thermal pressure, suggesting a magnetic field of  $\lesssim 35$   $\mu G$ , compatible with those observed in Galactic molecular clouds (Crutcher 1999).

## 5. Summary

Using *Spitzer* and *HST* observations of the superbubble N 51D in the LMC, we have identified three YSOs in dust globules. One of these is associated with an HH object that is detected outside the Galaxy for the first time. The SEDs of these YSOs are consistent with those of early-B stars with disk, envelope, and outflow cavities. The thermal pressure of the dust globule is much lower than that of the surrounding warm photoionized gas or the hot shock-heated gas in the superbubble interior. If star formation is induced by the thermal pressure of the hot gas, the magnetic field of the dust globule is  $\lesssim 35$   $\mu G$ .

This work is supported by the grant JPL-1264494.

## REFERENCES

Allen, L. E., et al. 2004, ApJS, 154, 363

- Breysacher, J., Azzopardi, M., & Testor, G. 1999, *A&AS*, 137, 117
- Chen, C.-H. R., Chu, Y.-H., Gruendl, R. A., & Points, S. D. 2000, *AJ*, 119, 1317
- Chu, Y.-H., Chang, H.-W., Su, Y.-L., & Mac Low, M.-M. 1995, *ApJ*, 450, 157
- Chu, Y.-H., & Mac Low, M.-M. 1990, *ApJ*, 365, 510
- Clemens, D. P., Yun, J. L., & Heyer, M. H. 1991, *ApJS*, 75, 877
- Cooper, R. L., Guerrero, M. A., Chu, Y.-H., Chen, C.-H. R., & Dunne, B. C. 2004, *ApJ*, 605, 751
- Crutcher, R. M. 1999, *ApJ*, 520, 706
- Diolaiti, E., Bendinelli, O., Bonaccini, D., Close, L., Currie, D., & Parmeggiani, G. 2000, *A&AS*, 147, 335
- Dunne, B. C., Points, S. D., & Chu, Y.-H. 2001, *ApJS*, 136, 119
- Gordon, K. D., et al. 2005, *PASP*, 117, 503
- Fazio, G., et al. 2004, *ApJS*, 154, 10
- Garnett, D. R., Walsh, J. R., Chu, Y.-H., & Lasker, B. M. 1999, *AJ*, 117, 1285
- Henize, K. G. 1956, *ApJS*, 2, 315
- Hester, J. J., et al. 1996, *AJ*, 111, 2349
- Jones, T. J., Woodward, C. E., Boyer, M. L., Gehrz, R. D., & Polomski, E. 2005, *ApJ*, 620, 731
- Lucke, P. B., & Hodge, P. W. 1970, *AJ*, 75, 171
- Oey, M. S. 1996, *ApJS*, 104, 71
- Oey, M. S., & Smedley, S. A. 1998, *AJ*, 116, 1263
- Rieke, G., et al. 2004, *ApJS*, 154, 25
- Reipurth, B., & Bally, J. 2001, *ARA&A*, 39, 403
- Smith, R. C., and the MCELS team 1999, in *IAU Symp.* 199, p.28
- Whitney, B. A., Wood, K., Bjorkman, J. E., & Cohen, M. 2003, *ApJ*, 598, 1099

Whitney, B. A., et al. 2004, ApJS, 154, 315

Zaritsky, D., Harris, J., Thompson, I. B., Grebel, E. K., & Massey, P. 2002, AJ, 123, 855



Table 1. Spectral Energy Distribution of Three YSOs in N 51D<sup>a</sup>

Wavelength ( $\mu\text{m}$ )	Source 1 Flux (mJy)	Source 2 Flux (mJy)	Source 3 Flux (mJy)
3.6	$4.16 \pm 10\%$	$1.51 \pm 10\%$	$2.14 \pm 10\%$
4.5	$9.35 \pm 10\%$	$1.44 \pm 10\%$	$2.35 \pm 10\%$
5.8	$24.7 \pm 10\%$	$4.71 \pm 10\%$	$5.35 \pm 10\%$
8.0	$47.6 \pm 10\%$	$11.4 \pm 10\%$	$13.3 \pm 10\%$
24	$356 \pm 10\%$	$43 \pm 10\%$	$20 \pm 10\%$
70	$1508 \pm 20\%$	$429 \pm 20\%$	$180 \pm 20\%$
160	$1402 \pm 20\%$	$<193$	$<193$

<sup>a</sup>The errors are dominated by uncertainties in the flux calibration, as given in the IRAC and MIPS Data Handbooks. The measurement errors are only 2–3% for sources 1 and 3, and 4–7% for source 2.

Fig. 1.— *(a)* A color composite of N 51D with  $H\alpha$  in green, green continuum in blue, and IRAC  $8\ \mu\text{m}$  in red. The  $H\alpha$  and green continuum images are from the Magellanic Cloud Emission-Line Survey (Smith et al. 1999). *(b)* An IRAC color composite of N 51D with  $3.6\ \mu\text{m}$  in blue,  $4.5\ \mu\text{m}$  in green, and  $8.0\ \mu\text{m}$  in red.

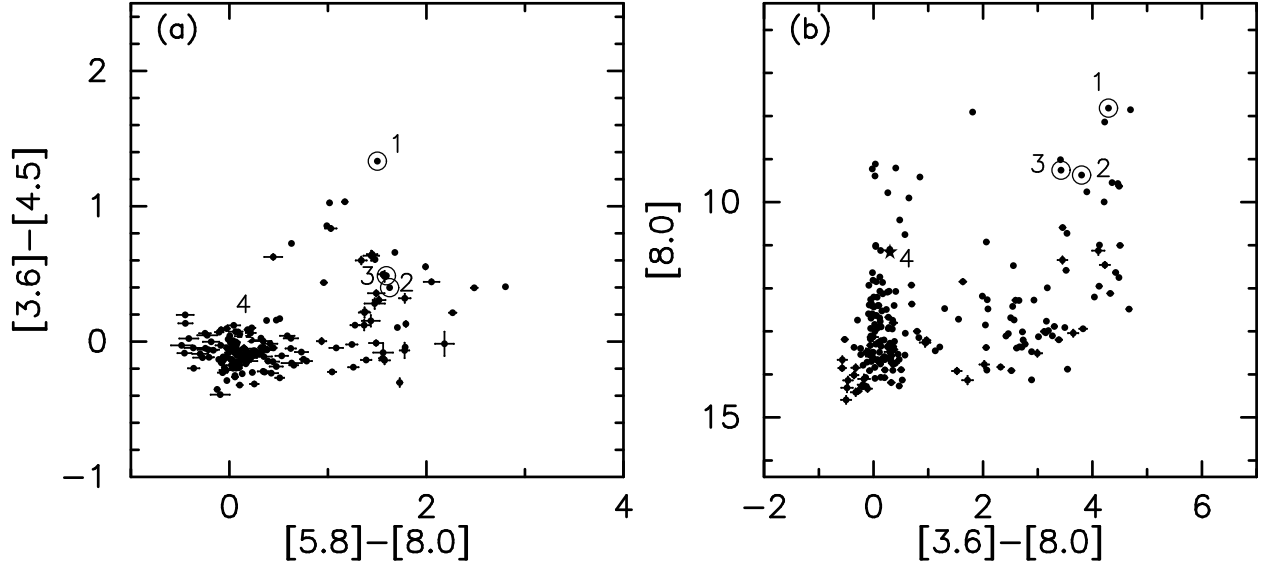


Fig. 2.— (a)  $[3.6]-[4.5]$  versus  $[5.8]-[8.0]$  color-color diagram of N 51D. (b)  $[8.0]$  versus  $[3.6]-[8.0]$  color-magnitude diagram of N 51D. Objects 1–3 are marked by circles around the data points, and object 4 is marked by a star symbol.

Fig. 3.— (a) A color composite of *HST* and *Spitzer* images of N 51D with  $H\alpha$  in green,  $[S\ II]$  in blue, and  $8.0\ \mu\text{m}$  in red. Note that the *Spitzer*  $8\ \mu\text{m}$  image has a  $\sim 2''$  resolution so the sources appear as smudges, as opposed to sharp point sources in the *HST* images. (b) *HST* WFPC2  $H\alpha$  image of YSO-1 and YSO-2. (c) *HST* WFPC2  $H\alpha$  image of YSO-3. (d) *HST* WFPC2  $[S\ II]$  image of YSO-3.

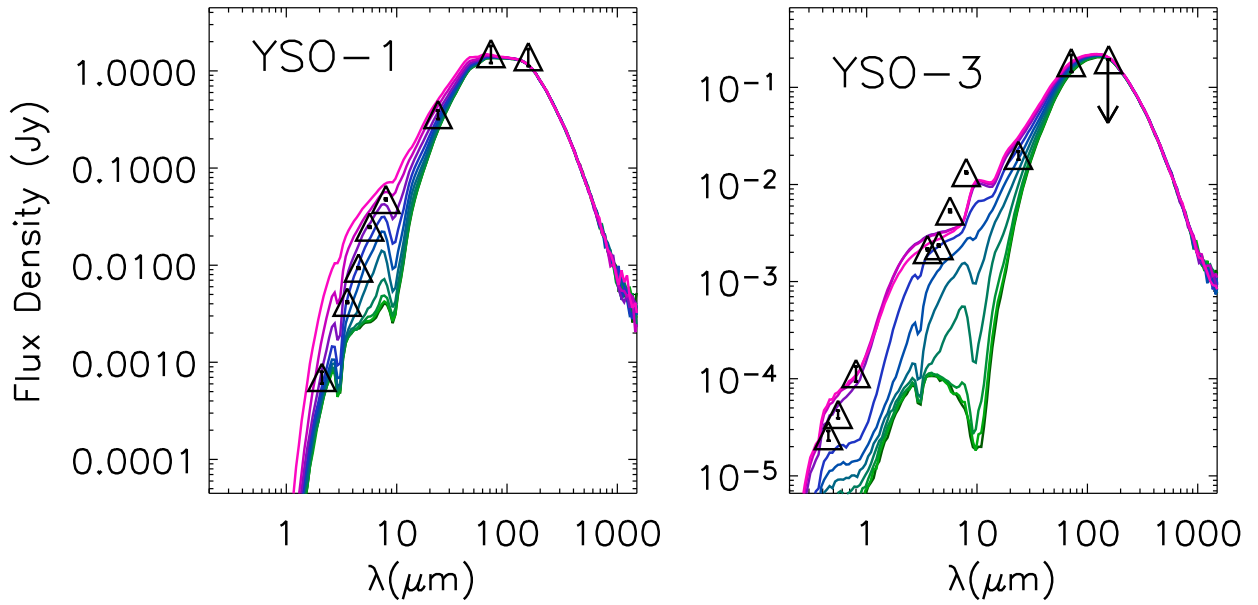


Fig. 4.— Models of SEDs for YSO-1 (*left*) and YSO-3 (*right*). The different colored lines correspond to different inclinations ranging from  $\cos i = 0.05$  (green) to 0.95 (pink) in steps of 0.1. The observations are shown as triangles with error bars.

This figure "f1.jpg" is available in "jpg" format from:

<http://arxiv.org/ps/astro-ph/0511505v2>

This figure "f3.jpg" is available in "jpg" format from:

<http://arxiv.org/ps/astro-ph/0511505v2>